

Metering Error Estimation of Fast-Charging Stations Using Charging Data Analytics

Kang Ma, Xiulan Liu, Xi Chen, Xiaohu Liu, Wei Zhao, Lisha Peng, *Senior Member, IEEE*,
Songling Huang, *Senior Member, IEEE*, Shisong Li, *Senior Member, IEEE*

Abstract—Accurate electric energy metering (EEM) of fast charging stations (FCSs), serving as critical infrastructure in the electric vehicle (EV) industry and as significant carriers of vehicle-to-grid (V2G) technology, is the cornerstone for ensuring fair electric energy transactions. Traditional on-site verification methods, constrained by their high costs and low efficiency, struggle to keep pace with the rapid global expansion of FCSs. In response, this paper adopts a data-driven approach and proposes the measuring performance comparison (MPC) method. By utilizing the estimation value of state-of-charge (SOC) as a medium, MPC establishes comparison chains of EEM performance of multiple FCSs. Therefore, the estimation of EEM errors for FCSs with high efficiency is enabled. Moreover, this paper summarizes the interfering factors of estimation results and establishes corresponding error models and uncertainty models. Also, a method for discriminating whether there are EEM performance defects in FCSs is proposed. Finally, the feasibility of MPC method is validated, with results indicating that for FCSs with an accuracy grade of 2%, the discriminative accuracy exceeds 95%. The MPC provides a viable approach for the online monitoring of EEM performance for FCSs, laying a foundation for a fair and just electricity trading market.

Index Terms—fast charging station, electric energy metering, data-driven analytics, SOC, electric vehicle.

I. INTRODUCTION

AS an environmentally-friendly means of transportation, the electric vehicle (EV) is crucial for addressing the prominent issues faced by humanity, that is, the shortage of fossil fuels and climate change [1], [2]. As shown in Fig. 1, the EV industry has achieved rapid development globally. In order to alleviate the ‘range anxiety’ of EV users and promote the further development of the EV industry, governments around the world have accelerated the construction of infrastructure such as charging stations [3], [4]. Among them, DC charging stations (also known as fast charging stations, FCSs) have been favored by EV users due to the high charging power. Moreover, as an important carrier of vehicle-to-grid (V2G) technology, the FCS is an indispensable device in future distributed grid [5]–[7]. According to the statistical data of the International Energy Agency (IEA), by the end of 2023, the number of publicly available fast charging points worldwide has reached 1.4 million. Including the United States, China, and the European Union, major

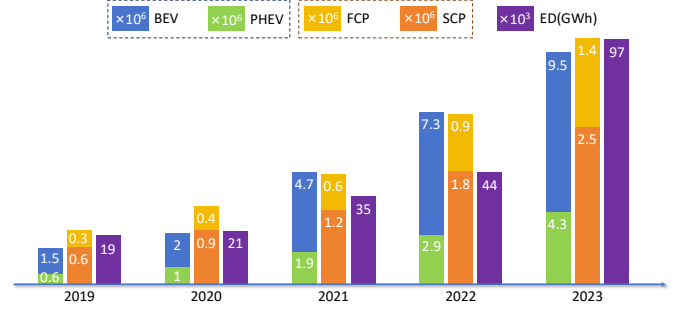


Fig. 1. Worldwide statistical data of EV industry, including the sales number of battery electric vehicles (BEV) and plug-in hybrid electric vehicles (PHEV), the number of publicly available fast charging points (FCP) and slow charging points (SCP), and the electricity demand (ED, GWh) by the end of 2023.

EV-using countries have almost established a complete fast charging service system. Behind the large-scale FCSs is a huge electricity trading market. The accuracy of EEM at FCS is related to the immediate interest of power grid companies and EV users. Especially for power grid companies, inaccurate EEM will cause massive energy waste and economic losses. Therefore, the accurate EEM value of FCSs is the only way to avoid disputes between power grid companies and EV users.

Due to the impact of complex operating environments and components aging, the EEM error of FCSs is inevitable. Therefore, it is necessary to regularly verify the EEM accuracy of FCSs to guide the calibration work. In China, FCSs have been included in the metering instruments subject to mandatory verification (verification period not exceeding 3 years). As a consequence, domestic research on EEM error verification technology of FCSs started earlier, with the development of field calibrator of EEM error beginning in the 2010s. According to the load type, the field verification is divided into real-load and virtual-load verification [8]. The real-load or virtual-load field calibrator with high accuracy of EEM is used to meter the same load as the FCS being verified. By comparing the EEM values, the EEM error of the FCS is calculated by

$$\gamma = \frac{E_1 - E_0}{E_0} \times 100\%, \quad (1)$$

where E_1 is the EEM value of the FCS, and E_0 is the EEM value of the field calibrator. Compared to the real-load verification, the virtual-load verification divides the voltage and current into different circuits, thereby not generating any electric energy loss. Therefore, from the perspective of energy conservation, virtual-load verification has advantages. Domes-

Kang Ma, Xiaohu Liu, Wei Zhao, Lisha Peng, Songling Huang, and Shisong Li are with the Department of Electrical Engineering, Tsinghua University, Beijing 100084, China. Xiulan Liu and Xi Chen are with the Electric Power Research Institute, State Grid Beijing Electric Power Company, Beijing 100045.

Email: shisongli@tsinghua.edu.cn

tic scholars have focused their research on the development of field calibrators, aiming to improve hardware and software performance to enhance their intelligence, portability, and anti-interference capabilities. Overseas, in light of the rapid increase in the number of EVs and FCSs, the National Institute of Standards and Technology (NIST) initiated a research project in March 2023 on the development of field calibrator for EEM accuracy of FCSs. Meanwhile, many countries have successively started research on laboratory verification techniques for DC energy meters, and are actively promoting the formulation of relevant laws and regulations [9].

To ensure the accuracy of field verification results, the EEM value of the field calibrator should not be too small, which leads to disadvantages of high time cost and low efficiency. According to on-site experience, the verification duration for an FCS is approximately 30 minutes. Therefore, the field verification method cannot meet the verification needs of massive FCSs. In view of that, the scholars are also actively exploring remote verification methods. The existing technical proposal involves using a multi-channel switching device to remotely switch the connection of the field calibrator and a cluster of FCSs, thereby achieving remote verification of EEM accuracy [10]. However, like the field verification method, this method essentially belongs to a ‘point-to-point’ approach, whose inherent drawbacks of high time cost and low efficiency remain unavoidable.

It is worth noting that the dilemmas faced in EEM error verification of FCSs also exist in accuracy verification of electric meters [11]–[13], voltage transformers [14], current transformers [15], [16], and other meters in the power system. In these fields, scholars have introduced data-driven methods to monitor the accuracy of field meters, thereby saving the verification costs. Specifically, within the topological framework of the power grid, electrical topology connections have been established between different meters, and the theoretical model of the relationships between the measurement values is established. Based on this theoretical model, combined with big data of measurement, the measurement accuracy can be evaluated. Here, the question is can we establish the electrical topology relationship of different FCSs? Based on the measurement data of EVs and FCSs, this paper establishes comparison chains for the EEM performance between multiple FCSs by using the state-of-charge (SOC) value estimated by EVs’ battery management system (BMS) as an intermediary. Lastly, the EEM errors of multiple FCSs are estimated by the method of metering performance comparison (MPC). Specifically, assuming that the capacity of the EV’s battery pack is stable and the SOC estimation is accurate. For every 1% increase in SOC, the corresponding charging energy value remains constant. Here, this value is defined as battery pack energy density (BPED), i.e.

$$E_d = \frac{E}{\Delta\text{SOC}}, \quad (2)$$

where E is the charging energy, ΔSOC is the change value of SOC, with the scale of %. Hence, when an EV is charged at FCS-A, the EEM value of FCS-A is E_A , and the change value of SOC is ΔSOC_A . Subsequently, when the same EV

is charged at FCS-B, the EEM value of FCS-B is E_B , and the change value of SOC is ΔSOC_B . The relative EEM error of FCS-B to FCS-A is given by

$$\begin{aligned} \gamma_{B \rightarrow A} &= \frac{E_{dB} - E_{dA}}{E_{dA}} \\ &= \frac{\frac{E_B}{\Delta\text{SOC}_B} - \frac{E_A}{\Delta\text{SOC}_A}}{\frac{E_A}{\Delta\text{SOC}_A}} \times 100\%. \end{aligned} \quad (3)$$

So far, the electrical topology between multiple FCSs has been established. Combined with the big data of EVs charging, the EEM errors of multiple FCSs can be estimated.

The remaining sections of this paper are organized as follows: Section II introduces the principles of the MPC method, Section III investigates the interfering factors affecting the accuracy of the estimation results, Section IV provides the estimation algorithm and analyzes the uncertainty of the estimation results, Section V conducts the validation of the estimation model, and Section VI presents the conclusions of this paper.

II. PRINCIPLE OF THE PROPOSED DATA-DRIVEN METERING ERROR ESTIMATION METHOD

As mentioned in Section I, the principle of the MPC method for EEM errors of FCSs is shown in Fig. 2. Under the premise that the capacity of the EV’s battery pack is stable and the SOC estimation is accurate, according to big data of EVs charging records, reference charging stations (RCSs) are selected, and the EEM error of RCSs is estimated first. Then, multiple comparison chains are built with the beginning of RCSs. For Equation (3), assuming that the EEM error of FCS-A is γ_A , the EEM error of FCS-B is given by

$$\gamma_B = \gamma_{B \rightarrow A} + \frac{E_{dB}}{E_{dA}} \gamma_A. \quad (4)$$

Herein, the EEM errors of all FCSs are calculable. Presently, the question is how to select the RCSs. As shown in Fig. 3(a), according to the on-site statistical data, the EEM errors of FCSs follow a normal distribution with an average value of 0. For one charging record of an EV charging at a FCS, the relationship between the estimation and true value of BPED is depicted as

$$\hat{E}_{di} = (1 + \gamma_i) E_d, \quad (5)$$

where \hat{E}_{di} is the estimation value, E_d the true value and γ_i the EEM error of the FCS- i . Hence, when the same EV has charging records at multiple FCSs, the average value of BPED estimation is

$$\hat{E}_d = E_d + \frac{\sum_{i=1}^n \gamma_i}{n} E_d. \quad (6)$$

n is the number of FCSs. Ideally, as long as n is large enough, the value of $\sum_{i=1}^n \gamma_i$ will infinitely approach 0, that is the estimation value will infinitely approach the true value. Furthermore, the EEM errors of these FCSs can be fixed according to Equation (5), and these FCSs can be considered as RCSs. However, the reality is that few FCSs serve the same EV. Most likely, it will lead to a significant error in the

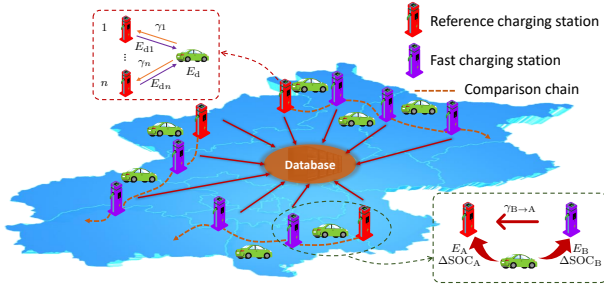


Fig. 2. Principle of the estimation method for FCSs' EEM accuracy based on charging data.

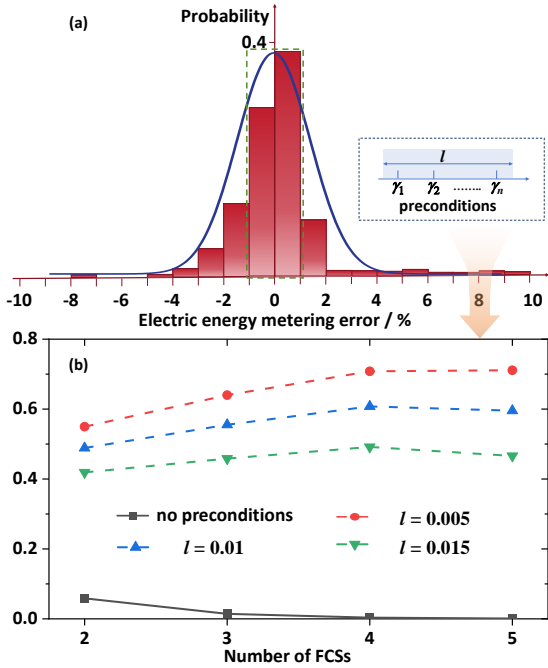


Fig. 3. Determination of the RCSs. (a) is the normal distribution of EEM error of on-site FCSs. The number of FCSs is 3500 produced by 10 manufacturers. According to the fitting result, the average value of this normal distribution is approximately 0, and the standard deviation equals 1.62%. (b) is the probability of EEM errors in FCSs cluster. The horizontal coordinate represents the number of FCSs in the cluster, and the vertical coordinate represents the probability that the EEM errors of all FCSs are within the range of $[-0.01, 0.01]$. Different curves represent the probability under different preconditions.

estimation value of BPED. To address this issue, we need to add some screening criteria for FCSs to improve the estimation accuracy of the BPED.

Actually, it is expected to select a cluster of FCSs with EEM errors close to 0. By utilizing the charging records of an EV at this cluster of FCSs, a more accurate estimation of BPED can be obtained. According to Fig. 3(b), if no preconditions are added, the probability that the EEM errors of n -FCS cluster are all within the range of $[-\gamma_0, \gamma_0]$ is quite small. Therefore, the precondition that the relative EEM errors between any two FCSs in the cluster is smaller than a specific value l is added to improve such probability. As shown in Fig. 3(b), such probability is significantly improved under this precondition, especially when l is small. In practice, by

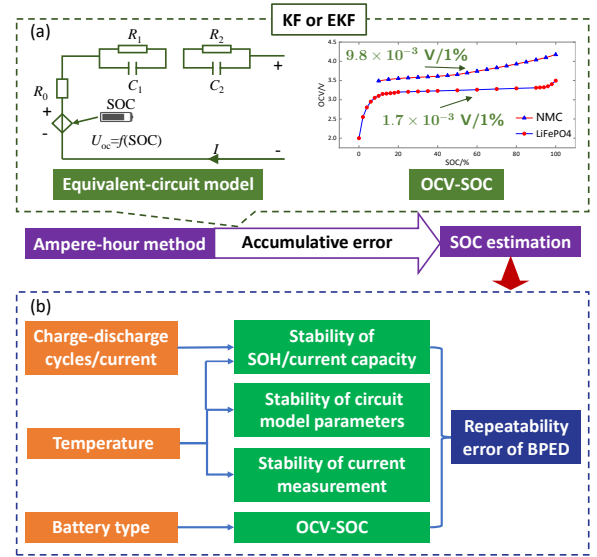


Fig. 4. (a) is the method based on KF or EKF. In which, the state equations are obtained according to the equivalent-circuit model and OCV-SOC curve [21]. The accumulative error of the ampere-hour method is compensated. (b) is the interfering factor on the repeatability error of BPED, including the stability of state-of-healthy (SOH)/current capacity, circuit model parameters, current measurement, and the characteristics of OCV-SOC curve. Moreover, the stability of SOH/current capacity is primarily influenced by the number of charge-discharge cycles and temperature. The stability of circuit model parameters is primarily affected by temperature variations. The stability of current measurement is dependent on the stability of the onboard current sensor, which is mainly influenced by temperature drift. The OCV-SOC curve is determined by the intrinsic characteristics of the battery. Generally speaking, the OCV-SOC curve characteristics of different battery types exhibit significant deficiencies.

selecting the appropriate value of l and the size of the FCSs cluster, the suitable cluster can be selected and the EEM errors of RCSs can be fixed by the aforementioned method.

So far, the EEM errors of large-scale FCSs can be estimated by utilizing the big data of charging records, ideally. But in reality, the capacity of EV's battery pack is time-variant. Meanwhile, the accurate estimation of SOC is a very challenging task due to the high nonlinearity of EV's battery system. Hence, the data pre-processing is vital to accurate estimation. Afterward, the interfering factors of estimation accuracy are analyzed, and the method of data pre-processing is introduced.

III. INTERFERING FACTORS OF ESTIMATION ACCURACY

A. Repeatability error of BPED

In the MPC method, the constancy of BPED serves as a prerequisite for establishing accurate comparison chains. According to Equation (2), the stability of BPED, which refers to the capacity to maintain equal changes in SOC when the charging/discharging energy is the same, is closely related to the SOC estimation algorithm and status of the battery pack. To date, the SOC estimation algorithms currently used in EV products are primarily based on the Kalman filter/extended Kalman filter (KF/EKF) [17]–[19]. As shown in Fig. 4(a). The KF/EKF method is grounded in the ampere-hour (Ah) method. The equation of the Ah method is given by [20]

$$\text{SOC}(t) = \text{SOC}(t_0) + \frac{1}{C_r \times \text{SOH}} \int_{t_0}^{t_0+t} I d(\tau), \quad (7)$$

where $\text{SOC}(t_0)$ is the SOC value at initial state. C_r is the rated capacity. SOH is the state-of-health of the battery pack, which is defined as the ratio of the current capacity to the rated capacity. I is the charging current. Owing to the absence of calibration and feedback mechanisms in the Ah method, cumulative errors progressively accumulate over time, leading to a significant deviation of the estimated value from the true value. To mitigate the cumulative errors, the KF or EKF is employed to rectify the estimation result of the Ah method. According to Fig. 4 (b), the repeatability error of BPED is affected by the number of charge-discharge cycles, temperature, and battery type. Specifically,

① Charge-discharge cycles/current:

The variation of lithium-ion battery (the most common battery type for EVs) capacity with the number of charge-discharge cycles is studied in [22]. The capacity of the onboard battery pack gradually decreases with the increase of charge-discharge cycles. Nonetheless, when the cycle number is less than 500, the decay in battery capacity is less than 0.2 % per every 100 cycles. Therefore, in order to mitigate or avoid the impact of charge-discharge cycles, an upper limit should be set for the time interval of charging data used in the estimation model.

The impact of charging current on the capacity is studied in [23] and [24]. Usually, the capacity will decrease with the increase of charging current. Especially, in low (below 20 °C) and high (above 40 °C) temperature environments, the impact of charging current is more severe.

In addition, the charging current will affect the conversion efficiency. The conversion efficiency is defined as the ratio of the actual charging capacity to the EEM value of the FCS. Due to the existence of line losses in the cable of the charging gun, the conversion efficiency is typically less than 1. By equating the cable to a resistor, the conversion efficiency is given by

$$\eta = \left(1 - \frac{IR}{U}\right) \times 100\%. \quad (8)$$

Where U represents the charging voltage, I represents the charging current, and R represents the resistance value of the cable. Subsequently, when evaluating the uncertainty, it is necessary to take into account the influence of conversion efficiency.

② Temperature:

According to Fig. 4 (b), the influence of temperature includes:

1) SOH/current capacity

Existing research has demonstrated that ambient temperature is a significant factor affecting the capacity of on-board battery packs [23]–[26]. Referring to [23] and [24], when the temperature is below 20 °C, the capacity reduction of lithium-ion batteries is more severe. While the temperature exceeds 40 °C, the capacity exhibits a slight decline.

2) Circuit model parameters

Currently, battery models encompass electrochemical models and equivalent-circuit models. Considering the trade-offs between simulation accuracy, complexity, and parameter identification difficulty, equivalent-circuit models have become commonly used battery models in SOC estimation algorithms, particularly the 2-order Thevenin model. As illustrated in Fig. 4 (a), The parameters of the 2-order Thevenin model include: the ohmic internal resistance (R_0), the polarization resistances (R_1 and R_2), and the polarization capacitors (C_1 and C_2). According to reference [27], a decrease in temperature leads to a significant increase in the ohmic resistance value. The value of R_0 at -10 °C is twice of that at 25 °C. Moreover, with variations in temperature, both the polarization resistances and the polarization capacitance values undergo substantial fluctuations.

3) Current measurement

The accuracy of the Ah method is highly dependent on the measurement accuracy of the sensors within the battery pack, particularly the current sensors. Considering the space utilization and reliability requirements of EVs, onboard battery packs typically require current sensors that are compact, cost-effective and have strong anti-interference capabilities. Commonly used sensors include Hall-effect current sensors and shunt resistors. These sensors are designed with temperature considerations and incorporate corresponding compensation measures, allowing their temperature coefficients to be controlled within 0.1%/°C [28].

③ Battery type:

Lithium-ion batteries employed in EVs encompass various types, including LiNiMnCoO₂ (NMC) batteries, NCA batteries, LiFePO₄ batteries, and etc [29], [30]. These batteries exhibit differences in energy density, cycling performance, and safety characteristics. It's noted that the characteristics of OCV-SOC curve for different types is different. The OCV-SOC curves for NMC batteries and LiFePO₄ batteries are shown in Fig. 4 (a). Due to the flat region in the middle segment of the OCV-SOC curve for LiFePO₄ batteries, the prediction of SOC by OCV method will result in significant errors. Consequently, in the MPC method, to ensure the accuracy of comparison chains, the charging data from LiFePO₄ batteries is not recommended.

In summary, the stability of BPED is subject to numerous interference factors, and the mechanisms are complex, making it difficult to establish a theoretical model for repeatability errors. Consequently, the repeatability error of BPED is quantified through experimental methods. Here, two EVs from different manufacturers are selected as experimental subjects and multiple charging tests are conducted on the two EVs. The distribution characteristics of BPED values for the two test EVs are statistically analyzed, separately.

As shown in Fig. 5, the BPED values of the test EVs exhibit the normal distribution. For EV1, within the statistical interval, the range of charging current varies from 42.8 to 44.5 A, the average temperature of the battery pack is 28.5 °C. According to the fitting results, the mean value of BPED is 0.34 kWh, and the standard deviation is 0.017 kWh. For EV2, the charging

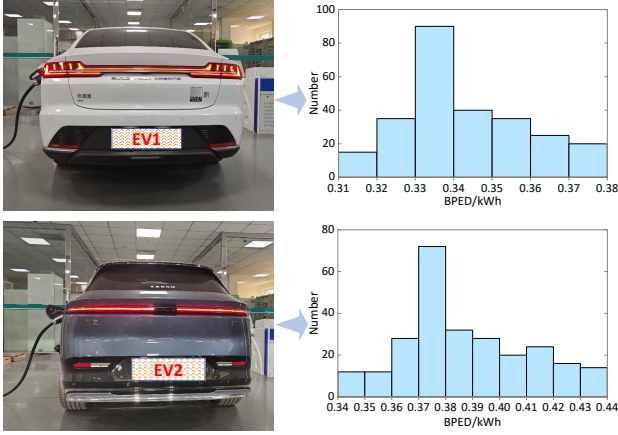


Fig. 5. Experimental results. The charging mode of the test FCS is constant current. The resistance value of the charging gun is 3 mΩ. Before the charging test, the SOC of test EVs is controlled under 10%. For each test Ev, the number of charging-discharging cycles is 3.

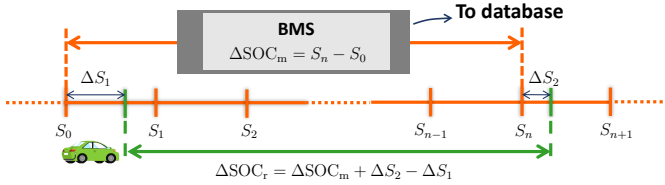


Fig. 6. Schematic diagram of SOC quantization error. The green line represents the real change of SOC, whereas the orange line denotes the change of SOC as calculated by the BMS.

current ranges from 39.7 to 43.4 A, the average temperature of the battery pack is 29.4 °C. The mean value of BPED is 0.38 kWh, and the standard deviation is 0.022 kWh. That is, the relative repeatability error of BPED is less than 6%.

B. Quantization error of SOC

In reality, the sampling frequency of operational FCSs doesn't exceed 1/60 Hz, and the resolution of SOC in the onboard BMS is only 1%, which leads to quantization error of SOC. As illustrated in Fig. 6, the D-value between ΔSOC_r and ΔSOC_m is referred to the SOC quantization error. Assuming the charging energy is E , the estimation error of the BPED due to the SOC quantization error is given by

$$e = \frac{E_{dm} - E_{dr}}{E_{dr}} = \frac{\Delta S_2 - \Delta S_1}{S_n - S_0} \times 100\% \quad (9)$$

Typically, the change in SOC is less than 90% during the EV charging. The value of $\Delta S_2 - \Delta S_1$ is a random variable distributed within the interval $(-1, 1)$. Consequently, the error in BPED estimation caused by the SOC quantization error is higher than 2%, which can't be ignored. In light of this, a probability model for the SOC quantization error is established. Assuming that ΔS_1 and ΔS_2 follow a uniform distribution over an interval $[0, 1)$, the probability density function is given by

$$f_{\Delta S}(x) = \begin{cases} 1, & 0 \leq x < 1 \\ 0, & \text{others} \end{cases} \quad (10)$$

Meanwhile, ΔS_1 and ΔS_2 are mutually independent. Thus, the probability distribution for the quantization error $y = \Delta S_2 - \Delta S_1$ is given by

$$f_Y(y) = \int_{-\infty}^{+\infty} f_{\Delta S_1}(x) f_{\Delta S_2}(y+x) dx = \begin{cases} 1+y, & -1 < y < 0 \\ 1-y, & 0 \leq y < 1 \\ 0, & \text{others} \end{cases} \quad (11)$$

Furthermore, assuming that the data points uploaded by the FCS are represented as $[(S_0, E_0), (S_1, E_1), \dots, (S_n, E_n)]$, the true value of BPED should satisfy the inequalities:

$$\begin{cases} \frac{E_1 - E_0}{S_1 - S_0 + 1} \leq E_d \leq \frac{E_1 - E_0}{S_1 - S_0 - 1} \\ \frac{E_2 - E_0}{S_2 - S_0 + 1} \leq E_d \leq \frac{E_2 - E_0}{S_2 - S_0 - 1} \\ \dots \\ \frac{E_n - E_0}{S_n - S_0 + 1} \leq E_d \leq \frac{E_n - E_0}{S_n - S_0 - 1} \end{cases} \quad (12)$$

By solving the aforementioned system of inequalities, the range of the true value of BPED is obtained as $[E_{d \min}, E_{d \max}]$. Thereby, the range of the quantization error is scaled to $[\frac{E}{E_{d \max}} - (S_n - S_0), \frac{E}{E_{d \min}} - (S_n - S_0)]$. Let $y_{\min} = \frac{E}{E_{d \max}} - (S_n - S_0)$, $y_{\max} = \frac{E}{E_{d \min}} - (S_n - S_0)$, under the prior condition, the conditional probability density function of the SOC quantization error $f_{y|(y_{\min} \leq y \leq y_{\max})}(y)$ can be obtained.

Herein, having considered the SOC quantization error, the value of BPED should be given by the unbiased estimation instead of Equation (2). The unbiased estimation is given by Equation (13), which is detailed in Table I.

$$E(E_d) = \int_{y_{\min}}^{y_{\max}} \frac{E}{S_n - S_0 + y} f_{y|(y_{\min} \leq y \leq y_{\max})}(y) dy \quad (13)$$

In which,

$$y_0 = S_n - S_0, \quad (14)$$

$$a = (y_{\max} - y_{\min})(2 + y_{\max} + y_{\min}), \quad (15)$$

$$b = (y_{\max} - y_{\min})(2 - y_{\max} - y_{\min}), \quad (16)$$

$$c = 2(y_{\max} - y_{\min}) - (y_{\max}^2 + y_{\min}^2). \quad (17)$$

IV. ESTIMATION ALGORITHM AND UNCERTAINTY ANALYSIS

A. Estimation algorithm

According to the aforementioned content, the EEM errors estimation algorithm for FCSs is as follows:

① Inputting the raw charging order data: The raw order data encompasses the charging process data for all FCSs, with the time span of charging orders not exceeding two months (Section III-A). The charging process data include at least the following items: time information, EEM value of the FCS, SOC, temperature, charging current, and voltage.

② Data pre-processing: The pre-processing includes the following steps:

1) For the same EV, the charging process data of each charging order is grouped by charging current to form

TABLE I
DETAILS OF EQUATION (13) AND (22)

Condition	Equation		Ref
$y_{\max} < 0$	$E(E_d) = \frac{2E}{a}$	$y_{\max} - y_{\min} + (1 + y_0) \ln \frac{y_{\max} + y_0}{y_{\min} + y_0}$	(13-A)
	$E(E_d^2) = \frac{2E^2}{a}$	$\frac{1 + y_{\min}}{y_0 + y_{\min}} - \frac{1 + y_{\max}}{y_0 + y_{\max}} + \ln \frac{y_0 + y_{\max}}{y_0 + y_{\min}}$	(22-A)
$y_{\min} > 0$	$E(E_d) = \frac{2E}{b}$	$y_{\min} - y_{\max} + (1 + y_0) \ln \frac{y_{\max} + y_0}{y_{\min} + y_0}$	(13-B)
	$E(E_d^2) = \frac{2E^2}{b}$	$\frac{1 + y_0}{y_0 + y_{\min}} - \frac{1 + y_0}{y_0 + y_{\max}} + \ln \frac{y_0 + y_{\min}}{y_0 + y_{\max}}$	(22-B)
$y_{\max} > 0$ and $y_{\min} < 0$	$E(E_d) = \frac{2E}{c}$	$(1 + y_0) \ln \frac{y_{\max} + y_0}{y_0} + (1 - y_0) \ln \frac{y_0}{y_{\min} + y_0} - y_{\min} - y_{\max}$	(13-C)
	$E(E_d^2) = \frac{2E^2}{c}$	$1 + \frac{1 + y_{\min}}{y_0 + y_{\min}} - \frac{1 + y_0}{y_0 + y_{\max}} + \ln \frac{y_0}{y_0 + y_{\max}} + \ln \frac{y_0}{y_0 + y_{\min}}$	(22-C)

charging data segments, which will be used for the subsequent identification of RCSs and comparison chains. In each charging data segment, the peak-to-peak value of the charging current does not exceed the set threshold, ΔI (Section III-A).

- 2) Exclude charging data segments with an average temperature below 20 °C or above 40 °C (Section III-A).
- 3) Exclude charging data segments with the SOC-change-value less than the set threshold to reduce the impact of SOC quantization error (Equation (9)).
- 4) Exclude charging data segments related to EVs with poor stability of expected BPED. Herein, an evaluation method for the stability of expected BPED is introduced. To eliminate the impact of FCSs, charging data segments from the same EV and the same FCS are employed for the stability evaluation. Specifically, if the number of charging data segments is n . The stability is characterized by the relative repeatability error, i.e.:

$$\delta = \frac{\sqrt{\frac{\sum_i (E_{di} - \bar{E}_d)^2}{n-1}}}{\bar{E}_d}. \quad (18)$$

E_{di} represents the expected value of the BPED corresponding to the i -th charging data segment, which is calculated by Equation (13). \bar{E}_d denotes the average value of E_{di} . It is noteworthy that this data processing initiative is of paramount importance. During the operation, some battery cells of an EV may sustain damage, which can significantly impair the performance of the battery pack. Furthermore, some manufacturers have commenced the provision of battery replacement services, resulting in the same EV exhibiting entirely different battery pack performance across different time periods. Consequently, this data processing measure effectively mitigates substantial fluctuations in BPED caused by the aforementioned phenomena.

③ Identification of the RCSs: According to the method mentioned in Section II, the RCSs are determined and the EEM errors are calculated by Equation (5). In order to maintain the battery pack state as similar as possible, the D-value of the average charging current and temperature between charging data segments must be less than the predefined threshold.

④ Identification of the comparison chains: The starting point of each comparison chain is the RCS, and no FCS is

repeated within each comparison chain. The termination conditions for comparison chains are as follows: a) the length of the comparison chain reaches the maximum allowable value, and b) a RCS (other than started RCS) appears. Moreover, the D-value of the average charging current and temperature between the two charging data segments used in Equation (3) and (4) must be less than the predefined threshold.

⑤ EEM error calculation and uncertainty estimation: The EEM error of a FCS in comparison chain is calculated according to Equation (4). The uncertainty estimation method is detailed and introduced in Section IV-B.

B. Uncertainty analysis

In order to facilitate the subsequent discussion, as shown in Fig. 7, this section illustrates the uncertainty components in the MPC method by using an example with 3 vehicles and 5-FCSs. For a pair of EV-FCS (connected by a blue arrow), there are two charging data segments. For EV-1 and FCS-A, it is assumed that the corresponding EEM values of the FCS-A for the two charging data segments are denoted as E_{A1-1} and E_{A1-2} , respectively. While the changes of SOC measured by the BMS are denoted as ΔSOC_{A1-1} and ΔSOC_{A1-2} , respectively. The recording method for the remaining charging data segments follows the same pattern. Furthermore, based on the charging process data, the range of the SOC quantization error is narrowed down to $[y_{\min}, y_{\max}]$. Referring to Equation (13), the expected values of BPED are as given by

$$E_{dA1-1} = \eta_{A1-1} E'_{dA1-1} = \eta_{A1-1} \int_{y_{\min}}^{y_{\max}} \frac{E_{A1-1}}{\Delta SOC_{A1-1} + y} f_{y|(y_{\min} \leq y \leq y_{\max})} dy, \quad (19)$$

$$E_{dA1-2} = \eta_{A1-2} E'_{dA1-2} = \eta_{A1-2} \int_{y_{\min}}^{y_{\max}} \frac{E_{A1-2}}{\Delta SOC_{A1-2} + y} f_{y|(y_{\min} \leq y \leq y_{\max})} dy. \quad (20)$$

η_{A1-1} and η_{A1-2} are conversion efficiency. The uncertainty for E_{dA1-1} and E_{dA1-2} encompass the estimation error for conversion efficiency (UNC-1), SOC quantization error (UNC-2) and the repeatability error of BPED (UNC-3). Consequently, the assessment of the uncertainty components is developed.

- 1) Estimation error for conversion efficiency: According to the investigation results, the resistance of the connection cable is approximately 2.2 m Ω (for a length of 5 m).

And the contact resistance at the cable connections is about 0.1 mΩ. The charging voltage of FCSs can exceed 400 V, and the charging current typically remains below 200 A. Consequently, the conversion efficiency of FCSs is higher than 99.88%. In light of this, within the MPC model, the conversion efficiency of charging stations is set to 1, with a relative estimation error of approximately 0.2%.

- 2) SOC quantization error: Referring to the SOC quantization error model established in Section III-B, the Type-B uncertainty assessment method is employed, which utilizes the standard deviation of E'_{dA1-1} and E'_{dA1-2} to characterize the uncertainty component arising from the SOC quantization error. The standard deviation of E_{dA1-1} is given by

$$\sigma_1(E'_{dA1-1}) = \sqrt{E(E'^2_{dA1-1}) - E^2(E'_{dA1-1})}. \quad (21)$$

In which, $E(E'^2_{dA1-1})$ is calculated by

$$E(E'^2_{dA1-1}) = \int_{y_{\min}}^{y_{\max}} \left(\frac{E_{dA1-1}}{\Delta \text{SOC}_{A1-1} + y} \right)^2 f_{y|l}(y_{\min} \leq y \leq y_{\max}) dy. \quad (22)$$

The details of the integration are shown in Table I. Thus, $\sigma_1(E'_{dA1-1})$ can be calculated, so as $\sigma_1(E'_{dA1-2})$

- 3) Repeatability error of BPED: The TyAn uncertainty assessment method is employed. According to tests in Section III-A, the relative standard deviation of BPED is below 6%. However, the average values are used in Equation (19) and (20), hence, the uncertainty component of E_{dA1-1} and E_{dA1-2} arising from BPED repeatability error is given by

$$\sigma_2(E'_{dA1-1}) = \frac{\text{std}(\text{BPED})E'_{dA1-1}}{\sqrt{\Delta \text{SOC}_{A1-1}}}, \quad (23)$$

$$\sigma_2(E'_{dA1-2}) = \frac{\text{std}(\text{BPED})E'_{dA1-2}}{\sqrt{\Delta \text{SOC}_{A1-2}}}. \quad (24)$$

In which, $\text{std}(\text{BPED})$ is the relative uncertainty of BPED.

Here, the comprehensive uncertainties of E'_{dA1-1} and E'_{dA1-2} are given by

$$\sigma(E'_{dA1-1}) = \sqrt{(\sigma_1^2(E'_{dA1-1}) + \sigma_2^2(E'_{dA1-1}))}, \quad (25)$$

$$\sigma(E'_{dA1-2}) = \sqrt{(\sigma_1^2(E'_{dA1-2}) + \sigma_2^2(E'_{dA1-2}))}. \quad (26)$$

Furthermore, the uncertainties of E_{dA1-1} and E_{dA1-2} are given by

$$\sigma(E_{dA1-1}) = E_{dA1-1} \sqrt{\sigma_{r-cv}^2 + \frac{\sigma(E'_{dA1-1})^2}{(E'_{dA1-1})^2}}, \quad (27)$$

$$\sigma(E_{dA1-2}) = E_{dA1-2} \sqrt{\sigma_{r-cv}^2 + \frac{\sigma(E'_{dA1-2})^2}{(E'_{dA1-2})^2}}, \quad (28)$$

where σ_{r-cv} the relative uncertainty of the onversion efficiency. The BPED of EV-1, determined by FCS-A, is given by

$$E_{dA1} = \frac{E_{dA1-1} + E_{dA1-2}}{2}. \quad (29)$$

Therefore, the uncertainty for E_{dA1} is given by

$$\sigma(E_{dA1}) = \sqrt{\frac{\sigma(E_{dA1-1})^2 + \sigma(E_{dA1-2})^2}{4}}. \quad (30)$$

Herein, employing the same computational methodology, the value of $\sigma(E_{dA2})$, $\sigma(E_{dB1})$, and etc. can be calculated.

Subsequently, the RCSs need to be identified. As shown in Fig. 7, EV-1 has charging records at FCS-A, FCS-B, and FCS-C. Consequently, by utilizing the charging data, it is feasible to estimate the true value of BPED of EV-1. Assuming that the relative EEM errors of the three FCSs do not exceed l , and that their EEM errors are distributed within the interval of $[-\frac{l}{2}, \frac{l}{2}]$, the estimated value of BPED is given by

$$E_{d1} = \frac{E_{dA1} + E_{dB1} + E_{dC1}}{3}. \quad (31)$$

Therefore, the uncertainty of E_{d1} is given by

$$\sigma(E_{d1}) = \sqrt{\frac{\sigma(E_{dA1})^2 + \sigma(E_{dB1})^2 + \sigma(E_{dC1})^2}{3}}. \quad (32)$$

In addition, due to the normal distribution of the errors of FCSs, the estimation error of BPED (UNC-3) should not be neglected. According to Equation (6), the estimation error of E_{d1} is

$$e = \frac{\gamma_A + \gamma_B + \gamma_C}{3} E_{d10}. \quad (33)$$

In which, E_{d10} is the true value of EV-1's BPED. According to Fig. 3, the EEM of a FCS complies the normal distribution as indicated in

$$f_{\gamma}(x) = \frac{1}{\sqrt{2\pi}\sigma} e^{-\frac{x^2}{2\sigma^2}}. \quad (34)$$

Under the aforementioned conditions, the probability density of γ_A , γ_B and γ_C is given by

$$f_{\gamma|l}(x) = \begin{cases} \frac{f_{\gamma}(x)}{\int_{-\frac{l}{2}}^{\frac{l}{2}} f_{\gamma}(x) dx}, & -\frac{l}{2} \leq x \leq \frac{l}{2} \\ 0, & \text{others} \end{cases}. \quad (35)$$

Therefore, the uncertainty component arising from the estimation error of E_{d10} is given by

$$\sigma(e) = \frac{\sigma \sqrt{\text{erf}\left(\frac{l}{2\sqrt{2}\sigma}\right)}}{\sqrt{3}d} E_{d10}. \quad (36)$$

Furthermore, the EEM error of the RCS-A is given by

$$\gamma_A = \frac{E_{dA1} - E_{d10}}{E_{d10}} = \frac{E_{dA1}}{E_{d1} - e} - 1. \quad (37)$$

Apparently, the contributors to the error of γ_A encompass the errors of E_{dA1} , E_{d1} and e . Owing to the non-linear relationship of these variables, it is challenging to directly employ Equation (37) to establish the uncertainty relationship

between γ_A and E_{dA1} , E_{d1} , e . Herein, Equation (37) is rewritten using Taylor series expansion at $(E_{dA1}^0, E_{d1}^0, e^0)$, i.e.

$$\begin{aligned} \gamma_A &= \gamma_A^0 + \frac{1}{E_{d1}^0 - e^0} (E_{dA1} - E_{dA1}^0) \\ &\quad - \frac{E_{dA1}^0}{(E_{d1}^0 - e^0)^2} (E_{d1} - E_{d1}^0) + \frac{E_{dA1}^0}{(E_{d1}^0 - e^0)^2} (e - e^0). \end{aligned} \quad (38)$$

E_{dA1}^0 and E_{d1}^0 are calculated by Equation (19) and (31), e^0 is assigned as 0. γ_A^0 is calculated by Equation (37). Thus, the uncertainty of γ_A can be expressed as

$$\begin{aligned} \sigma(\gamma_A) &= \text{sqrt} \left(\frac{\sigma(E_{dA1})^2}{(E_{d1}^0 - e^0)^2} + \frac{(E_{dA1}^0)^2 \sigma(E_{d1})^2}{(E_{d1}^0 - e^0)^4} + \right. \\ &\quad \left. \frac{(E_{dA1}^0)^2 \sigma(e)^2}{(E_{d1}^0 - e^0)^4} - \frac{2E_{dA1}^0}{(E_{d1}^0 - e^0)^3} \text{COV}(E_{dA1}, E_{d1}) \right). \end{aligned} \quad (39)$$

Due to the lack of independence between E_{dA1} and E_{d1} , it is necessary to take into account the covariance in Equation (39). Here,

$$\begin{aligned} \text{COV}(E_{dA1}, E_{d1}) &= \text{E}[(E_{dA1} - \text{E}(E_{dA1}))(E_{d1} - \text{E}(E_{d1}))] \\ &= \text{E}(E_{dA1}E_{d1}) - \text{E}(E_{dA1})\text{E}(E_{d1}). \end{aligned} \quad (40)$$

Substitute Equation (31) into Equation (40). In which,

$$\begin{aligned} \text{E}(E_{dA1}E_{d1}) &= \\ &= \frac{1}{3} \text{E}(E_{dA1}^2 + E_{dA1}E_{dB1} + E_{dA1}E_{dC1}). \end{aligned} \quad (41)$$

Generally speaking, the charging behaviors among different FCSs are mutually independent. Therefore, Equation (41) can be expanded as

$$\begin{aligned} \text{E}(E_{dA1}E_{d1}) &= \frac{1}{3} [\text{E}(E_{dA1}^2) + \\ &= \text{E}(E_{dA1})\text{E}(E_{dB1}) + \text{E}(E_{dA1})\text{E}(E_{dC1})]. \end{aligned} \quad (42)$$

In which,

$$\text{E}(E_{dA1}^2) = \sigma(E_{dA1})^2 + \text{E}(E_{dA1})^2. \quad (43)$$

Up to now, γ_A and $\sigma(\gamma_A)$ can both be calculated. So as γ_B , $\sigma(\gamma_B)$ and γ_C , $\sigma(\gamma_C)$. Then, by employing the comparison chains, the EEM errors of other FCSs can be calculated. In this case, by EV-2 and EV-3, a comparison chain FCS-C \leftrightarrow FCS-D \leftrightarrow FCS-E is established. Thus, the EEM errors for FCS-D and FCS-E are given by

$$\gamma_D = \frac{E_{dD2} - E_{dC2}}{E_{dC2}} + \frac{E_{dD2}}{E_{dC2}} \gamma_C, \quad (44)$$

$$\gamma_E = \frac{E_{dE3} - E_{dD3}}{E_{dD3}} + \frac{E_{dE3}}{E_{dD3}} \gamma_D. \quad (45)$$

Similar to the computation process of $\sigma(\gamma_A)$, the issue of nonlinear relationships arises in the computation processes of $\sigma(\gamma_D)$ and $\sigma(\gamma_E)$. By emulating Equation (38), Equation (44) is expanded in a Taylor series at $(E_{dD2}^0, E_{dC2}^0, \gamma_C^0)$,

$$\begin{aligned} \gamma_D &= \gamma_D^0 + \frac{1 + \gamma_C^0}{E_{dC2}^0} (E_{dD2} - E_{dD2}^0) + \\ &= \frac{(1 + \gamma_C^0) E_{dD2}^0}{(E_{dC2}^0)^2} (E_{dC2} - E_{dC2}^0) + \frac{E_{dD2}^0}{E_{dC2}^0} (\gamma_C - \gamma_C^0). \end{aligned} \quad (46)$$

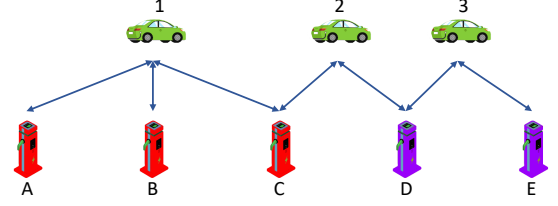


Fig. 7. An example for MPC method. Vehicles and piles connected by blue arrows indicate the presence of charging data segments.

Thus, the uncertainty of γ_D is given by

$$\begin{aligned} \sigma(\gamma_D) &= \text{sqrt} \left(\left(\frac{1 + \gamma_C^0}{E_{dC2}^0} \right)^2 \sigma(E_{dD2})^2 \right. \\ &= \left. + \left(\frac{(1 + \gamma_C^0) E_{dD2}^0}{(E_{dC2}^0)^2} \right)^2 \sigma(E_{dC2})^2 + \left(\frac{E_{dD2}^0}{E_{dC2}^0} \right)^2 \sigma(\gamma_C)^2 \right). \end{aligned} \quad (47)$$

The same methodology can be employed to calculate $\sigma(\gamma_E)$. At this juncture, the estimation of EEM errors for FCSs as well as the uncertainty associated with the estimation results are completed. Furthermore, it is imperative to discriminate whether there are EEM performance defects at FCSs. It is postulated that if the absolute value of EEM error is less than γ_t , the EEM error is deemed acceptable. Conversely, if the EEM error exceeds this threshold, it is considered unacceptable. Thus, the acceptable EEM error range is defined as $[-\gamma_t, \gamma_t]$. The MPC method is capable of delineating the distribution interval of the EEM error, namely $[\gamma_{FCS} - \sigma(\gamma_{FCS}), \gamma_{FCS} + \sigma(\gamma_{FCS})]$. Accordingly, this paper defines the probability of acceptable EEM error, which is defined as the ratio of the length of the EEM error distribution interval that falls within the acceptable EEM error range to the total length of the distribution interval. For instance, if $\gamma_{FCS} - \sigma(\gamma_{FCS}) < -\gamma_t$ and $-\gamma_t < \gamma_{FCS} + \sigma(\gamma_{FCS}) < \gamma_t$, the probability of acceptable EEM error is

$$P = \frac{\gamma_{FCS} + \sigma(\gamma_{FCS}) + \gamma_t}{2\sigma(\gamma_{FCS})} \times 100\%. \quad (48)$$

When this probability value exceeds 50%, the EEM error is deemed acceptable. Especially, when the EEM error distribution interval encompasses the acceptable range, that is, $\gamma_{FCS} - \sigma(\gamma_{FCS}) < -\gamma_t$ and $\gamma_{FCS} + \sigma(\gamma_{FCS}) > \gamma_t$, the estimation result is deemed unreliable.

V. ESTIMATION MODEL VALIDATION

Based on the principles elucidated in the preceding sections, this section employs field operational data to undertake the validation of the effectiveness of the MPC method. The charging data utilized in this section are derived from a subset of operational FCSs (with accuracy grade of 2%) located in North China. The timestamps of all charging data fall within March 2024. The dataset encompasses 7195 items of charging data, 567 FCSs, and 1274 EVs. The parameter settings in the estimated model are represented in Table II.

According to the MPC method, the number of RCSs is 423, among them, the number of RCSs possessed verification results is 73. The number of comparison chains is 294.

TABLE II
PARAMETERS OF THE ESTIMATION MODEL

Parameter	Value	Parameter	Value
Charging current threshold	4 A	Minimum Δ SOC	20%
Relative repeatability error of BPED	6%	Minimum number of FCSs (for RCSs)	3
Relative repeatability error threshold of expected BPED	1%	σ for EEM error distribution of FCS	1.62%
Relative EEM error threshold (for RCSs)	0.67%	Longest comparison chain	4 FCSs
D-temperature threshold	5 °C	Acceptable EEM error	$[-2\%, 2\%]$

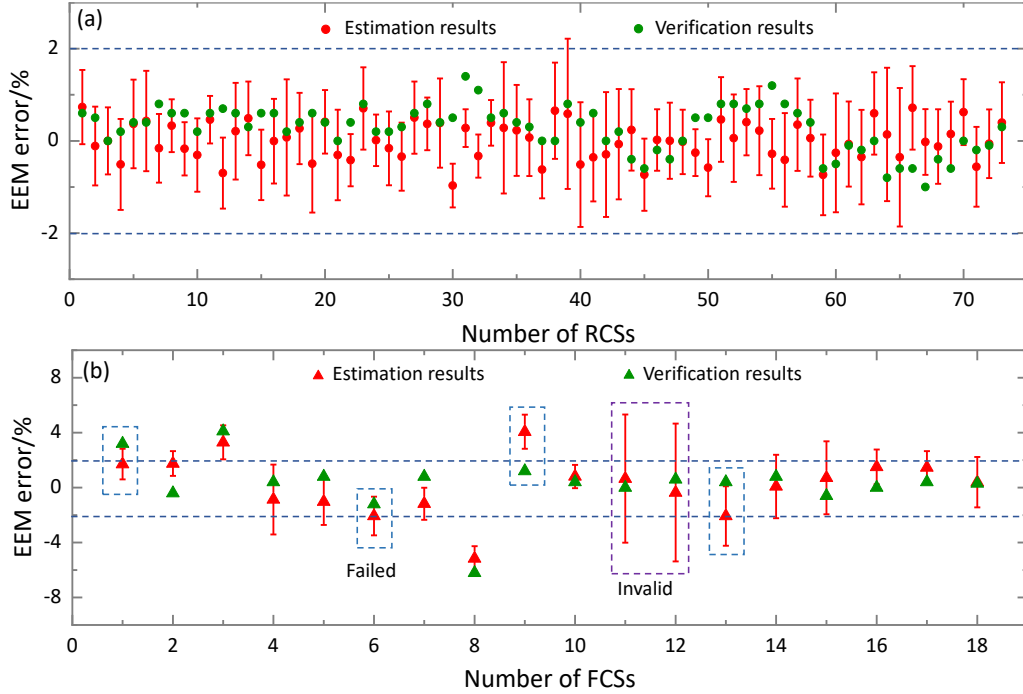


Fig. 8. A comparison between the estimation results and the verification results is presented, wherein (a) depicts the comparison for the RCSs, with 73 RCSs possessing verification results, and (b) illustrates the comparison for the other FCSs, with 18 FCSs having verification results.

The number of other FCSs with estimation results is 144, with 18 of them having verification results. The comparison between the estimation and verification results is shown in Fig. 8. Wherein, the EEM errors of all RCSs are estimated as acceptable, aligning perfectly with the verification results. For other FCSs, the estimation EEM errors for FCS-11 and FCS-12 exhibited large uncertainty, rendering the results invalid. The estimation EEM error for FCS-1 is deemed acceptable (with an expected EEM error of -1.7%, an uncertainty of 1.1%, and an acceptable probability of 63.1%), whereas the verification result is unacceptable (with a verification EEM error of 3.2%). The EEM errors of FCS-6, FCS-9, and FCS-13 are estimated as unacceptable (with expected EEM errors of -2.1%, -4.1%, and -2.1%, respectively, uncertainties of 1.4%, 1.2%, and 2.1%, and acceptable-probabilities of 47.6%, 0, and 48.3%, respectively), whereas their verification results are acceptable (with verification EEM errors of -1.2%, 1.2%, and 0.4%, respectively). The estimation conclusions for the remaining FCSs correspond with their verification conclusions.

VI. CONCLUSION

To overcome the drawbacks of high costs and low efficiency in existing on-site verification methods, this paper proposes

the MPC based on the concept of digital metrology. In MPC method, the comparison chains for EEM performance among multiple FCSs are established and mediated by SOC, enabling EEM error estimation of large-scale FCSs. Additionally, considering actual operational conditions, this paper summarizes the interfering factors of estimation results, including charge-discharge cycles, temperature, charging current, SOC estimation accuracy, and SOC quantization errors. The corresponding error models and uncertainty models are established. Also, a method for discriminating whether there are EEM performance defects is proposed. Finally, the feasibility of MPC method is validated, with results indicating that for FCSs with an accuracy grade of 2%, the discriminative accuracy exceeds 95%.

Looking ahead, with technological innovations in SOC estimation algorithms, there is potential for further enhancing the accuracy of SOC estimation. Moreover, the standardization of charging data in EV industry continues to strengthen. Hence, the accuracy of EEM error estimation can be improved further, facilitating more accurate online monitoring of large-scale FCSs for EEM performance. Ultimately, the MPC method is expected to promote the digital transformation of FCSs measurement verification.

REFERENCES

- [1] X. Lai, Y. Huang, C. Deng, H. Gu, X. Han, Y. Zheng, and M. Ouyang, "Sorting, regrouping, and echelon utilization of the large-scale retired lithium batteries: A critical review," *Renewable Sustainable Energy Rev.*, vol. 146, Art. no. 111162, Aug. 2021.
- [2] M. S. Mastoi, S. Zhuang, H. M. Munir, M. Haris, M. Hassan, M. Usman, S. S. H. Bukhari, and J.-S. Ro, "An in-depth analysis of electric vehicle charging station infrastructure, policy implications, and future trends," *Energy Rep.*, vol. 8, pp. 11504–11529, Nov. 2022.
- [3] J. Shi, W. Zhang, Y. Bao, D. W. Gao, and Z. Wang, "Load forecasting of electric vehicle charging stations: Attention based spatiotemporal multi graph convolutional networks," *IEEE Trans. Smart Grid*, vol. 15, no. 3, pp. 3016–3027, May. 2024.
- [4] M. Algafr, A. Alghazi, Y. Almoghathawi, H. Saleh, and K. Al-Shareef, "Smart city charging station allocation for electric vehicles using analytic hierarchy process and multiobjective goal-programming," *Appl. Energy*, vol. 372, Art. no. 123775, Oct. 2024.
- [5] J. Hu, C. Ye, Y. Ding, J. Tang, and S. Liu, "A distributed mpc to exploit reactive power v2g for real-time voltage regulation in distribution networks," *IEEE Trans. Smart Grid*, vol. 13, no. 1, pp. 576–588, Jan. 2022.
- [6] M. S. Mastoi, S. Zhuang, H. M. Munir, M. Haris, M. Hassan, M. Alqarni, and B. Alamri, "A study of charging-dispatch strategies and vehicle-to-grid technologies for electric vehicles in distribution networks," *Energy Rep.*, vol. 9, pp. 1777–1806, Dec. 2023.
- [7] H. An, J. Yi, Y. Xing, G. Zhang, O. Bamisile, J. Li, and Q. Huang, "A robust v2g voltage control scheme for distribution networks against cyber attacks and customer interruptions," *IEEE Trans. Smart Grid*, vol. 15, no. 4, pp. 3966–3978, Jul. 2024.
- [8] X. Li, L. Li, X. Liu, G. Yang, and Q. Zhou, "Verification scheme and system design of charging pile electric energy measurement," in *2018 4th International Conference on Environmental Science and Material Application (ESMA)*, Xian, China, Dec. 2018.
- [9] D. Herbst, M. Fuernschuss, P. Reichel, F. Lehfuss, C. Auer, and E. Schmautzer, "Challenges and related solutions for periodic verification of dc electric vehicle charging stations," in *IET Conference Proceedings*, vol. 2022, no. 3, pp. 113–117, Nov. 2022.
- [10] L. Yang, D. Zhang, G. Lin, Q. Song, Q. Meng, F. Pan, and C. Liu, "Research on remote calibration and online monitoring system of electric energy metering device," in *Journal of Physics: Conference Series*, vol. 1303, Art. no. 012119, May. 2019.
- [11] W. Luan, J. Peng, M. Maras, J. Lo, and B. Harapnuk, "Smart meter data analytics for distribution network connectivity verification," *IEEE Trans. Smart Grid*, vol. 6, no. 4, pp. 1964–1971, Jul. 2015.
- [12] Y. Wang, Q. Chen, T. Hong, and C. Kang, "Review of smart meter data analytics: Applications, methodologies, and challenges," *IEEE Trans. Smart Grid*, vol. 10, no. 3, pp. 3125–3148, May. 2019.
- [13] J. Duan, Q. Tang, J. Ma, and W. Yao, "Operational status evaluation of smart electricity meters using gaussian process regression with optimized-ard kernel," *IEEE Trans. Ind. Infomat.*, vol. 20, no. 2, pp. 1272–1282, Feb. 2024.
- [14] T. Lei, M. Faifer, R. Ottoboni, and S. Toscani, "On-line fault detection technique for voltage transformers," *Measurement*, vol. 108, pp. 193–200, Oct. 2017.
- [15] B. V. Djokic, H. Parks, N. Wise, D. Naumovic-Vukovic, S. P. Skundric, A. D. Zigic, and V. Poluzanski, "A comparison of two current transformer calibration systems at nrc canada," *IEEE Trans. Instrum. Meas.*, vol. 66, no. 6, pp. 1628–1635, Jun. 2017.
- [16] R. Morello, S. C. Mukhopadhyay, Z. Liu, D. Slomovitz, and S. R. Samantaray, "Advances on sensing technologies for smart cities and power grids: A review," *IEEE Sensors J.*, vol. 17, no. 23, pp. 7596–7610, Dec. 2017.
- [17] I. Hafez, A. Wadi, M. F. Abdel-Hafez, and A. A. Hussein, "Variational bayesian-based maximum correntropy cubature kalman filter method for state-of-charge estimation of li-ion battery cells," *IEEE Trans. Veh. Technol.*, vol. 72, no. 3, pp. 3090–3104, Mar. 2023.
- [18] X. Liu, Q. Li, L. Wang, M. Lin, and J. Wu, "Data-driven state of charge estimation for power battery with improved extended kalman filter," *IEEE Trans. Instrum. Meas.*, vol. 72, pp. 1–10, Jan. 2023.
- [19] Z. Zhang, L. Jiang, L. Zhang, and C. Huang, "State-of-charge estimation of lithium-ion battery pack by using an adaptive extended kalman filter for electric vehicles," *J. Energy Storage*, vol. 37, Art. no. 102457, May. 2021.
- [20] D. Huang, Z. Chen, C. Zheng, and H. Li, "A model-based state-of-charge estimation method for series-connected lithium-ion battery pack considering fast-varying cell temperature," *Energy*, vol. 185, pp. 847–861, Oct. 2019.
- [21] L. Ju, P. Long, G. Geng, and Q. Jiang, "Open circuit voltage- state of charge curve calibration by redefining max-min bounds for lithium-ion batteries," *J. Energy Storage*, vol. 79, Art. no. 110224, Feb. 2024.
- [22] K. A. Severson, P. M. Attia, N. Jin, N. Perkins, B. Jiang, Z. Yang, M. H. Chen, M. Aykol, P. K. Herring, D. Fraggedakis, M. Z. Bazan, S. J. Harris, W. C. Chueh, and R. D. Braatz, "Data-driven prediction of battery cycle life before capacity degradation," *Nat. Energy*, vol. 4, no. 5, pp. 383–391, May. 2019.
- [23] M. Dubarry, C. Truchot, B. Y. Liaw, K. Gering, S. Sazhin, D. Jamison, and C. Michelbacher, "Evaluation of commercial lithium-ion cells based on composite positive electrode for plug-in hybrid electric vehicle applications iii. effect of thermal excursions without prolonged thermal aging," *J. Electrochem. Soc.*, vol. 160, no. 1, pp. A191–A199, Feb. 2013.
- [24] X. Liu, Y. He, G. Zeng, and X. Zheng, "State-of-power estimation for li-ion battery considering the effect of temperature," *Transactions of China Electrotechnical Society*, vol. 31, no. 13, pp. 155–163, Oct. 2016.
- [25] T. Zhang, "Performance degradation and sealing failure analysis of pouch lithium-ion batteries under multi-storage conditions," *J. Power Sources*, vol. 613, Art. no. 234891, Sep. 2024.
- [26] W. Keyoonwong, K. Phipuannok, K. Janesawatpong, K. Seeboon-rueang, N. Amnuaysap, and T. Puttawong, "Study impedance and temperature behavior of lfp battery as function of relative humidity and temperature under various conditions," in *2024 10th International Conference on Engineering, Applied Sciences, and Technology (ICEAST)*, Luang Prabang, Laos, Jun. 2024.
- [27] J. Zhou, X. Sun, K. Liu, M. Wang, X. Yang, and G. Liu, "Research on the soc estimation algorithm of combining sliding mode observer with extended kalman filter," *Proceedings of the CSEE*, vol. 41, no. 2, pp. 692–702, Jan. 2024.
- [28] K. Zhu, X. Liu, and P. W. T. Pong, "Performance study on commercial magnetic sensors for measuring current of unmanned aerial vehicles," *IEEE Trans. Instrum. Meas.*, vol. 69, no. 4, pp. 1397–1407, Apr. 2020.
- [29] M. Hu, Y. Wang, and D. Ye, "A timely review of lithium-ion batteries in electric vehicles: Progress, future opportunities, and challenges," in *E3S Web of Conferences*, vol. 308, Art. no. 01015, Aug. 2021.
- [30] A. A. Pesaran, "Lithium-ion battery technologies for electric vehicles," *IEEE Electrification Mag.*, vol. 11, no. 2, pp. 35–43, Jun. 2023.